INTERNATIONAL JOURNAL OF PRECISION ENGINEERING AND MANUFACTURING Vol. 17, No. 4, pp. 503-510 APRIL 2016 / 503
DOI: 10.1007/s12541-016-0063-3 ISSN 2234-7593 (Print) / ISSN 2005-4602 (Online)

Stress and Surface Tension Analyses of Water on Graphene-Coated Copper Surfaces

Chinh Thanh Nguyen[1] and BoHung Kim[1,#]

1 School of Mechanical Engineering, University of Ulsan, 93, Daehak-ro, Nam-gu, Ulsan, 44610, South Korea
Corresponding Author / E-mail: bohungk@ulsan.ac.kr, TEL: +82-52-259-2705, FAX: +82-52-259-1680

KEYWORDS: Molecular dynamics simulation, Graphene coating, Water contact angle, Solid-liquid interface, Surface tension

Graphene-coated materials have recently emerged as promising materials for green renewable energy applications due to the benefits of combining graphene and metals. For these types of composites, the effect of graphene coating on the wettability of metal substrates has attracted much attention from researchers. In this paper, a series of molecular dynamics simulations, in which water droplets are deposited on bare Cu (111) and graphene-coated Cu (111), were conducted to investigate the influences of graphene coating on the wettability of copper. We found that water contact angles gradually increased and converged to the value measured on pure graphite surfaces as the number of graphene layers deposited on the Cu (111) surface increased. The "wetting transparency of graphene was proven to break down as demonstrated by the fact that the water contact angle of mono-layer graphene-coated copper was found to significantly increase as compared to that of bare copper. Density and stress profiles of water droplets were examined to confirm the effect of the number of graphene layers on copper-water interactions. We also examined the surface tensions of water droplets on graphene-coated copper substrates. We found that the liquid-vapor and solid-vapor surface tensions are constant while the solid-liquid tension varies with the graphene coating; this leads to the variation in the water droplet contact angles.

Manuscript received: April 15, 2015 / Revised: September 15, 2015 / Accepted: November 24, 2015
This paper was presented at ISGMA 2015

NOMENCLATURE

σ = Diameter of molecules (zero potential distance) (nm)
ε = Depth of LJ potential (eV)
r_c = cut-off distance (nm)
N = Number of molecules
ρ = Mass density (g/cm^3)
γ_{LV} = Liquid-vapor surface tension (mN/m)
γ_{SL} = Solid-liquid surface tension (mN/m)
γ_{SV} = Solid-vapor surface tension (mN/m)

1. Introduction

Graphene-coated metal materials have emerged as potential materials for the replacement of semiconductors, which are facing problems related to size reduction in the area of integrated circuit technologies. Currently, silicon materials used in semiconductors have nearly approached their size limit for satisfying the demands of increasing performance and the number of transistors per chip. Therefore, there has been much research focusing on the investigation of other materials for the replacement of silicon-based materials. Within this research trend, graphene has been particularly attractive because it possesses a number of unique properties. For example, a two-dimensional sheet of graphene is known to have high mechanical strength and high elasticity;[1] a single-graphene layer deposited on a silicon substrate was shown to greatly improve the electron mobility of the sample;[2] and graphene has high thermal conductivity, even when it is in contact with a substrate, making it is very useful in heat dissipation applications in nanoelectronics.[3] With these superior characteristics, nano-composites of graphene-coated metal substrates have the potential to be useful in circuit technologies and many other green renewable energy applications.

Among the significant effects that graphene has on metal substrates, the influence of graphene coating on the wetting behavior of substrates is extremely important. The wetting behavior is the key factor for understanding the van der Waals and electrostatic interactions between substrates and liquids, which are very influential on the thermal

behaviors at solid-liquid interfaces.[4-9] Nevertheless, the wetting properties of graphene-coated substrates have not been revealed completely. Rafiee et al. demonstrated that the wettability of substrates can be altered drastically, from superhydrophobic to superhydrophilic, by using graphene sheets.[10] By measuring contact angles, Wang et al. concluded that a graphene oxide sheet is hydrophilic and a pure graphene sheet is hydrophobic.[11] It was also shown by Zhou et al. that the epitaxial buffer layer (G_0) is more hydrophilic than subsequent layers (G_n); this is due to the increased perturbation of G_0 by the SiC substrate, surface defects, and functional groups.[12] Recently, both experiments and molecular dynamics simulations were conducted by Rafiee et al. to demonstrate that a single-layer graphene coating offers "wetting transparency to the underlying substrate (e.g., Cu, Au, or Si).[13] This means that coating only a single layer of graphene on these substrates does not change the water contact angle of the substrates. In other words, the van der Waals and electrostatic interactions between the substrates and water are not influenced by a single layer of graphene deposited on a substrate. This was considered to be an important study, demonstrating the great potential of graphene for a large number of applications. However, Shil et al. proved the breakdown of the "wetting transparency of graphene by showing that the wetting transparency fails significantly on superhydrophobic (contact angle > 90°) and superhydrophilic (contact angle < 30°) substrates.[14] Interestingly, Raij et al. also showed that the contact angle jumps significantly from 0° for bare copper to 70° for copper coated with one layer of graphene.[15] Subsequently, it was claimed by Shin et al. that the contact angle of monolayer graphene is constant at 90° independent of the underlying substrate.[16] Nevertheless, it was later argued by Shil et al. that the degree of wetting transparency of graphene depends on the specific substrate and that graphene is translucent to wetting.[17] In short, the complete physical explanation for the wetting behavior of graphene-coated substrates has yet to be concluded.

Be motivated by the current research situation in this topic, the objective of this paper is to study the wetting behavior of graphene-coated copper as the number of deposited graphene layers is increased. The contact angle values, density distributions, stress distributions, and surface tensions were analyzed to comprehend the effect of the graphene coatings on a copper substrate. Interestingly, the applicability of Young's equation is also investigated.

This paper is organized as follows: in section 2, we provide details on the MD simulations including a description of the simulation domains and a summary of the simulation parameters. In section 3, we discuss the results obtained regarding the density profiles, stress profiles, surface tensions, and contact angles. Finally, the conclusions are drawn in section 4.

2. MD Simulation Details and Theoretical Background

2.1 MD simulation details

A schematic diagram of the simulation is shown in Fig. 1. A drop of liquid water was placed on both a bare copper and a graphene-coated copper surface. The simulation dimensions were 16.35 × 16.07 × 17.41 nm in the $x \times y \times z$ directions, respectively. The dimensions of the solid substrate were chosen to be large enough so that the water droplet did not move out of the substrate border due to diffusion. The copper, formed by seven layers of Cu (111), was 1.25 nm in the z direction with an interlayer spacing of 2.084 Å. The number of graphene layers was changed from one to five, and the interlayer spacing between both graphene-graphene and copper-graphene was 3.4 Å. The height of the substrate was changed depending on the graphene thickness.

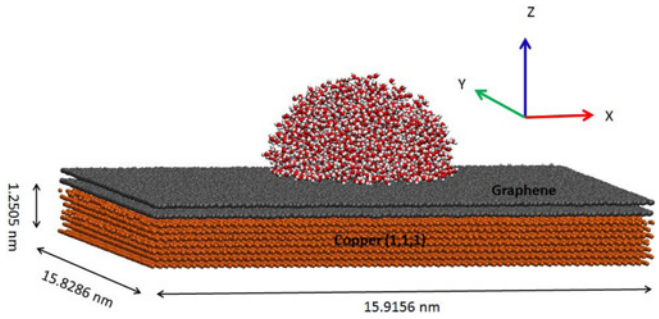

Fig. 1 3D schematic for MD simulation of a water droplet deposited on a graphene-coated copper (111) substrate

A Cu (111) surface structure was chosen as the substrate in this study because this structure matches best with graphene.[18] The growth of graphene on Cu (111) was previously achieved in an ultrahigh vacuum chamber.[19] The lattice constant of Cu (111) is 2.552 Å; the lattice constant of graphene was also chosen to be equal to 2.552 Å (although its original lattice constant was 2.46 Å). The reason for this choice is that with this lattice constant value, the honeycomb lattice structure of a graphene layer has the best match with the triangle-shaped lattice of Cu (111). It was shown that the atomic structure at the graphene-copper interface is sustainable and free from any defects or breakage of the graphene sheets.[20]

Simple point charge (SPC/E) model, which can be described as effective rigid pair potentials composed of Lennard-Jones (LJ) and Coulombic terms, was chosen to represent water molecules due to its simplicity and relatively low computational cost.[21] This model provides proper intermolecular interaction and polarization of the complex water structure. Also, another reason that the SPC/E model was chosen is because it provides the most accurate results for the orthobaric density and surface tensions,[22] which are the key factors that we examined in our study. This water model has three interaction sites, corresponding to the three atoms of water molecules. A point charge is assigned to each atom to model the long-range Coulombic interactions, and the oxygen atoms also exhibit LJ potential to model the van der Waals forces. Specifically, the oxygen and hydrogen atoms are assigned the partial charges $q_O = -0.8476$e and $q_H = 0.4238$e, respectively, to model the Coulombic interactions. A particle-particle particle-mesh (PPPM) was used to calculate the long-range electrostatic forces.[23] The harmonic O-H bond length (0.1 nm) and the H-O-H angle (109.47°) were kept rigid using the SHAKE algorithm.[24] LJ interactions were calculated between the wall molecules and the oxygen atoms of the liquid water. We use the truncated LJ (12-6) potential to model the van der Waals interactions, which is given as:

$$V_{truncated}(r_{ij}) = 4\varepsilon\left[\left(\left(\frac{\sigma}{r_{ij}}\right)^{12} - \left(\frac{\sigma}{r_{ij}}\right)^{6}\right) - \left(\left(\frac{\sigma}{r_c}\right)^{12} - \left(\frac{\sigma}{r_c}\right)^{6}\right)\right], \quad (1)$$

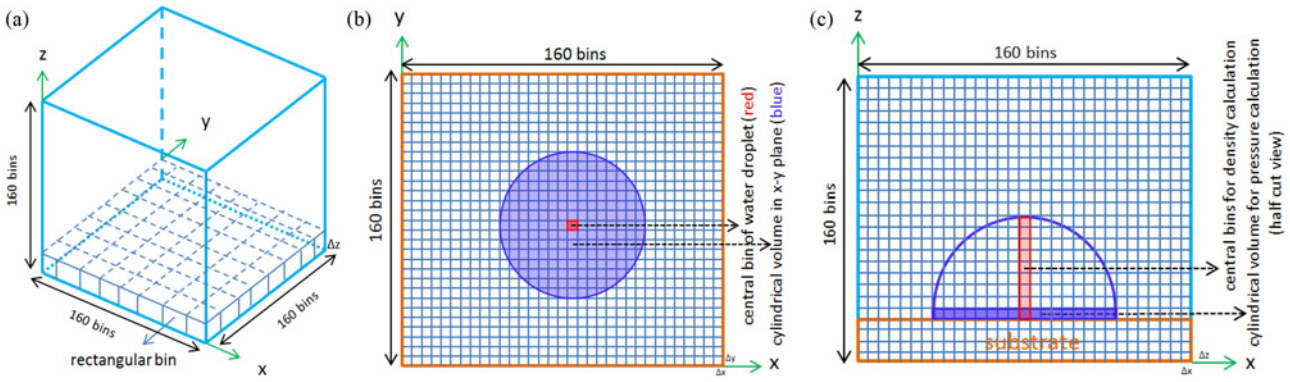

Fig. 2 (a) 3D bin division of the simulation domain; (b) Top view of a base x-y slab; (c) x-z plane cut-view along the droplet center inside the simulation domain

where ε is the depth of the potential well, σ is the molecular diameter, r_{ij} is the intermolecular distance, and r_c is the cut-off distance. Intermolecular forces were truncated at a cut-off distance of 15 Å, which is sufficiently large to account for long-range interactions.[8]

For the copper substrate, the many-body potential embedded atom method (EAM), which describes the total energy of a metal by calculating the embedding energy as a function of the atomic electron density, was used to model the intermolecular forces between Cu molecules.[25] The adaptive intermolecular reactive empirical bond-order (AIRBEO) potential was utilized to model the intermolecular interactions of C-C in the graphene layers.[26] The interactions of C-O and Cu-O were represented by the LJ potential. In particular, $\varepsilon_{C\text{-}O}$ = 0.00412 eV, $\sigma_{C\text{-}O}$ = 3.19 Å, $\varepsilon_{Cu\text{-}O}$ = 0.0114563 eV, and $\sigma_{Cu\text{-}O}$ = 2.75185 Å. The water droplet used in the simulations is nanometer-sized, so the contact angle is system-size dependent due to the effect of line tension at the tri-phase junction.[27] However, the main objective of this study is to investigate the wettability of the graphene-coated copper substrates through contact angles obtained in MD simulations using a fixed size of water droplet (2000 H2O molecules) to save computational cost. Therefore, the Cu-O interaction parameter was determined by conducting MD simulations to reproduce the macroscopic water contact angle of the pure copper substrate which was measured in the experiment.[13] The interactions between copper atoms and the carbon atoms of graphene layers were also represented by LJ potentials with $\varepsilon_{Cu\text{-}C}$ = 0.02578 eV and $\sigma_{Cu\text{-}C}$ = 3.0825 Å.[28]

All the simulations were started from the Maxwell-Boltzmann velocity distribution for all molecules at 300 K. The periodicity boundary condition was applied in the x and y directions. The NVT (constant number of molecules, constant volume, and constant temperature) ensemble was used initially with a Nose-Hoover thermostat, which maintained the system at 300 K. The time duration of the NVT ensemble was 1.0 ns to ensure that the system reaches isothermal steady state. The NVE (constant number of molecules, constant volume, and constant energy) ensemble was then used; the duration of the NVE ensemble was also 1.0 ns to ensure that the system reaches the equilibrium state. Time averaging data of the desired values was performed over the last 0.5 ns of the NVE. The computational domain was divided into rectangular bin structures in which there are 160 × 160 × 160 bins in three directions, as shown in Fig. 2(a). This number of bins was chosen so that each dimension of each bin is 1~2 Å; this is done to ensure that the data are collected properly. The simulation time step was set as 1.0 femtosecond (fs). All simulations were performed using LAMMPS.[29]

2.2 Density, stress, and surface tension determination

It was observed that the three-dimensional (3D) structure of a water droplet is spherical except in the region near the solid-liquid interface. Density values were calculated based on the central bins along the droplet center in the z direction and parallel with the substrate, as shown in Fig. 2(a) and 2(b). Due to the diffusion of the droplet on the surface, which can make the central bins change their locations, the locations of the central bins were shifted accordingly before the density data of the central bins were obtained.

The stress tensor profiles of water droplets on bare copper substrate and graphene-coated copper were investigated. S_{xx}, S_{yy}, and S_{zz} are the three mutually orthogonal components of normal stress tensors acting along the x, y, and z directions of the simulation domain, respectively. Both kinetic and virial stresses were included in these types of stresses; the kinetic component is the contribution from the linear momentum of particles while the virial component is an internal contribution from intermolecular forces between the particles. Also, because we worked with water, which has a complex molecular structure, the internal forces of the bonds and angles of water molecules must also be accounted for. The stress tensors were calculated based on the following formula:[30]

$$S_{\alpha\beta} = -\left(m v_\alpha v_\beta + \frac{1}{2}\sum_{m=1}^{N_p}(r_{1\alpha}F_{1\beta} + r_{2\alpha}F_{2\beta}) + \frac{1}{2}\sum_{n=1}^{N_b}(r_{1\alpha}F_{1\beta} + r_{2\alpha}F_{2\beta}) + \frac{1}{3}\sum_{n=1}^{N_a}(r_{1\alpha}F_{1\beta} + r_{2\alpha}F_{2\beta} + r_{3\alpha}F_{3\beta}) + Kspace(r_{i\alpha}, r_{i\beta}) + \sum_{n=1}^{N_f}(r_{i\alpha}, r_{i\beta}) \right), \quad (2)$$

where the first term on the right-hand side is the kinetic component, in which m is the atomic mass of particle i and v_α and v_β are the velocity components of particle i in the α and β directions. The second, third, fourth, and fifth terms are the virial component. The second term is a pairwise energy contribution where n loops over the N_p neighbors of atom i, r_1 and r_2 are the positions and F_1 and F_2 are the forces of the two atoms in the pairwise interaction. The third and fourth terms are the

bond and angle contributions for the N_b bonds and N_a angle, respectively, of which atom i is part of. The *Kspace* term is the contribution from the long-range Coulombic interactions for the PPPM solver. Finally, the fifth term is the SHAKE internal constraint force applied to particle i via the N_f fixes. In LAMMPS, the per-atom array values above are a product of the stress and volume units. Therefore, the actual local stress tensor in each rectangular bin was given by dividing the total per-atom stress tensor by the volume of each bin:

$$S_{\alpha\beta,rect} = \frac{S_{\alpha\beta} \times N_a}{V_{bin}}, \quad (3)$$

where $S_{\alpha\beta rect}$ is the actual local stress in a rectangular bin; N_a is the number of atoms per bin; and $V_{bin} = \Delta x \times \Delta y \times \Delta z$ where Δx, Δy, and Δz are the lengths of each rectangular bin in the x, y, and z directions. We aimed to investigate the local stress tensors of water along the z direction of the simulation domain; therefore, the simulation domain was divided into local regions with length Δz along the z direction. Because the water droplet structure is spherical, the local stress tensors of a water droplet in each Δz region were calculated based on the cylindrical volume. This volume was approximately structured by the rectangular bins that are part of the droplet in that z region, as shown in Fig. 2(a) and 2(b). The cylindrical volume was in the plane parallel with the x-y plane, and its height was Δz. The local stress tensor (in one direction) in each cylindrical volume was calculated as the average of all of the corresponding local stress tensors (in that direction) of the rectangular bins that constitute that cylindrical volume:

$$S_{\alpha\beta,cyl} = \frac{\Sigma S_{\alpha\beta,rect}}{N_{bin}}, \quad (4)$$

where $S_{\alpha\beta cyl}$ is a local stress tensor of cylindrical volume and N_{bin} is the number of rectangular bins that constitute the cylindrical volume.

Based on the normal stress components, the liquid-vapor surface tension (denoted as γ_{LV}) of a water droplet on a solid substrate was calculated using the following formula:[31]

$$\gamma_{LV} = \frac{L_z}{2}\left[\langle S_{zz,cyl}\rangle - \frac{1}{2}(\langle S_{xx,cyl}\rangle + \langle S_{yy,cyl}\rangle)\right], \quad (5)$$

where L_z is the height of the droplet and $S_{xx,cyl}$, $S_{yy,cyl}$, and $S_{zz,cyl}$ are the normal stress tensors in each cylindrical volume along the z direction of the simulation domain.

We also investigated the surface tension behavior at the boundaries between the solid-liquid and solid-vapor interfaces, denoted as γ_{SL} and γ_{SI}, respectively. These tension values can be calculated based on the Bakker's equation.[32] Using this, the surface tension of a flat interface normal to the z direction can be calculated from the difference of the stress components:

$$\gamma = \int [S_N(z) - S_T(z)]dz, \quad (6)$$

where γ is the solid-liquid or solid-vapor surface tension; $S_N = S_{xx,cyl}$; and $S_T = 1/2(S_{xx,cyl} + S_{yy,cyl})$. The integration range must cover the whole interface; therefore, the range of integration is determined based on the stress tensor profile of the water droplet.[33] For the solid-liquid surface tension, the integration range should be along the z direction from the solid-liquid interface to the point where the stress starts to converge to zero; this is defined as the "effecting region". In our cases, we found that this region should be from z = 0 to 11 Å. For the solid-vapor surface tension, the integration range should be outside of the liquid region; therefore, the starting integration point along the z direction was determined to be from 34 Å to 36 Å, depending on the graphene coating.

2.3 Contact angle calculation methods

Static contact angle is relevant for this study due to its role in representing the wettability of a solid surface.[34] We performed several methods to calculate the contact angles of water droplets on the various substrates. The first method, used to calculate contact angles from MD simulation snapshots, was based on the geometric method[35] proposed by M. Barisik et al. With this, the droplet boundary was determined to be the point at which the water density is half of the bulk value (0.5 g/cm^3). A circle was drawn along the boundary from the points 11 Å above the substrate to avoid the effects of density fluctuation at the solid-liquid interface. The contact angle θ was calculated based on a simple geometric formula, and then the time average of all of the water contact angles of a water droplet at equilibrium was obtained. The second method used to calculate contact angles was based on the Young's equation, which relies on surface tension values:

$$\gamma_{SV} = \gamma_{SL} + \gamma_{LV}\cos\theta. \quad (7)$$

In this method, the contact angle of a liquid drop on a solid surface is defined by the mechanical equilibrium of the drop under the action of the three surface tensions. This equation was proposed by Thomas Young over 150 years ago, and it has been well-known for determining the contact angle of a solid surface at the macro-scale. In this study, due to the capability of MD simulations in obtaining the surface tensions directly from the simulation data, we aimed to verify the applicability of the Young's equation at the nanoscale using the obtained surface tensions.

3. Results and Discussion

3.1 Density distribution, stress distribution, and surface tension analysis

Fig. 3(a) shows the density profiles of water droplets on all of the different graphene coated copper substrates. In the direction normal to the interface, the water density exhibited oscillations caused by interactions between the liquid and solid molecules. The density values converged to the value of 1.00 g/cm^3 in the bulk water and then gradually went to zero. The density build up near the substrate-water surface was due to the fact that the interaction strength between the substrate and the water is greater than the interaction strength of water-water; therefore, water molecules were attracted to the region near the surface and collided with the surface. Two distinct density peaks were observed for the bare copper and all of the other graphene-coated cases. Interestingly, when graphene layers were added to the bare copper substrate, the first density peaks of water near the graphene-coated substrates increased and were higher than that of bare copper, as shown in Fig. 3(b). This phenomenon can be explained by the fact that when graphene layers were added to the bare copper, the water molecules

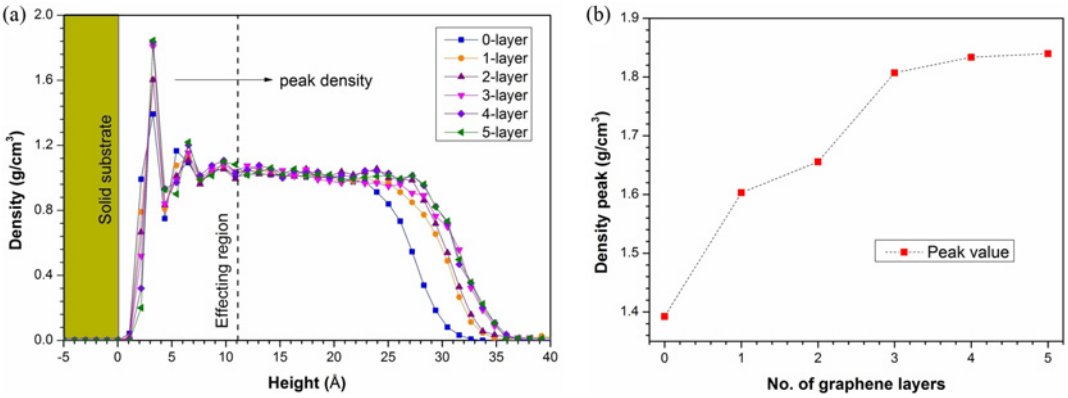

Fig. 3 (a) Density profiles of water droplet along the z-axis on various substrates; (b) Density peak values for various graphene-coated substrates

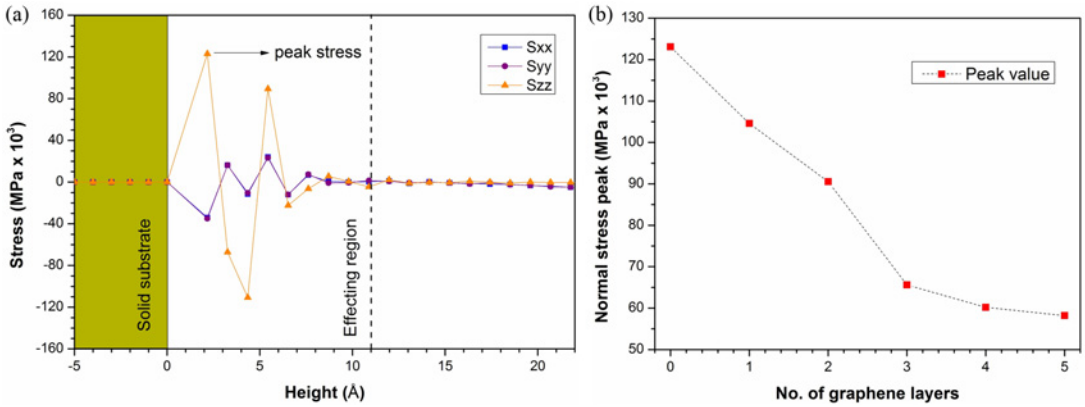

Fig. 4 (a) A typical stress distribution of water droplets on the solid substrates; (b) Normal stress peak values for various graphene-coated substrates

interacted with the carbon atoms of graphene, which has a solid-liquid intermolecular diameter that is higher than that of copper and water. This increase in the solid-liquid intermolecular diameter makes the amplitude of density variations larger;[36] therefore the density peak is higher. This is strong evidence suggesting that even a single graphene layer can change the solid properties of the substrate from those of copper to those of graphene. In other words, a single layer of graphene can change the material properties of the copper substrate significantly. We also observed a change in the height of the water droplet when more graphene layers were added to the copper substrate. The height of a droplet is defined as the point where the density goes to zero with a rapid decrease away from the surface.[35] Using this definition, the height of the droplets clearly increased when one graphene layer was added to the copper substrate. However, changes in droplet height were much less obvious for graphene coatings with two or more layers. Overall, the change in the density profile supports the fact that the solid-water interaction strength decreases when graphene layers are added to the copper substrate.

The oscillatory behavior of stress tensors at the solid-liquid interfaces can be seen in the stress tensor distributions. This oscillatory behavior is consistent with the behavior observed for the water density. Fig. 4(a) shows a typical distribution of stress tensors along the direction normal to the substrate. Additionally, the stress tensors converged to zero in the region outside of the "effecting region". Moreover, a decrease in the peak values of the normal stresses was observed when more graphene layers were coated on the copper substrates (Fig. 4(b)). The main reason for this is that as more graphene layers were added to the substrate, the interactions between the substrate and the liquid water decreased. This allowed the virial stresses at the interface to decrease because virial stresses are directly related to intermolecular interaction between molecules. This change in the stress profiles provided evidence that the graphene coating affects the interaction strength between copper substrates and water droplets.

Fig. 5(a) shows the values of the liquid-vapor surface tensions for the different types of graphene coatings. We can see that the liquid-vapor surface tensions of the water droplets were largely unchanged as graphene layers were added to the copper substrate. The liquid-vapor surface tensions fluctuated around a mean value 70.6 mN/m. This result is only slightly different from the typical value for water (72 mN/m). Fig. 5(b) shows the values of γ_{SL} and γ_{SV} for the various types of graphene coatings. It was found that the solid-liquid surface tension increased as the thickness of the graphene coating increased, converging to a stable value after four layers of graphene. The reason is that the decrease in the solid-liquid interaction strength led the liquid-liquid interaction to gradually become more dominant, which caused an increase in the solid-liquid surface tension. Importantly, the observation

Table 1 Surface tensions and contact angles (in degree) of water droplets on various substrates

Case	γ_{LV} (mN/m)	γ_{SL} (mN/m)	γ_{SV} (mN/m)	θ-Geom.	θ-Y. Eq.	θ-Exp.
Bare copper	70. 6±1.7	19.28	0	86.1	105.22	85.9
Mono-layer		46.76		92.2	133.47	86.2
Two-layer		54.60		93.7	142.37	86.5
Three-layer		58.87		94.8	150.93	86.6
Four-layer		61.60		95.9	152.67	88.3
Five-layer		62.96		96.1	156.32	90.6

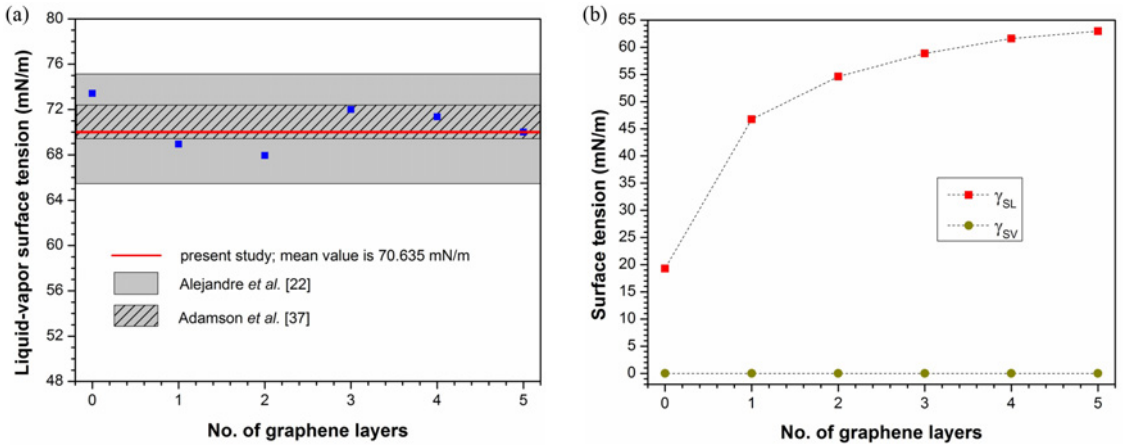

Fig. 5 (a) Liquid-vapor surface tension for various cases of graphene coating; (b) Solid-liquid and solid-vapor surface tensions for various cases of graphene coating

that the solid-liquid surface tension is increased significantly with only a single graphene layer supports the idea that monolayer graphene can cause a remarkable reduction in the interaction strength between a copper substrate and water. We also found that the solid-vapor surface tensions, for all cases, were approximately equal to zero. This result implies that graphene coating has no effect on the solid-vapor surface tension.

3.2 Water contact angles obtained from different methods

Fig. 6 shows the contact angle values obtained from the different methods (also shown in Table 1). For the geometric method, we observed that the contact angle of a water droplet on the monolayer graphene-coated copper substrate was much higher compared to bare copper, increasing from 86.1° to 92.2°. This important phenomenon suggests that there is no wetting transparency when one layer of graphene is deposited on copper. Importantly, the contact angle of water droplets approached the value of pure graphite after the deposition of four layers of graphene. These contact angles are quite different from the experimental results provided by Rafiee et al..[13] The geometric MD results showed no wetting transparency for monolayer graphene while the experimental contact angles changed by only a small amount, even with graphene coatings of up to three layers. However, the increasing tendency of the contact angles was the same; the contact angles gradually approached the value of pure graphite, although there was a small difference in the convergence values, which may be caused by non-ideal effects in the experiments that were not modeled in the simulations. Interestingly, the values obtained from the Young's equation did not match the geometric MD values as well as the experimental

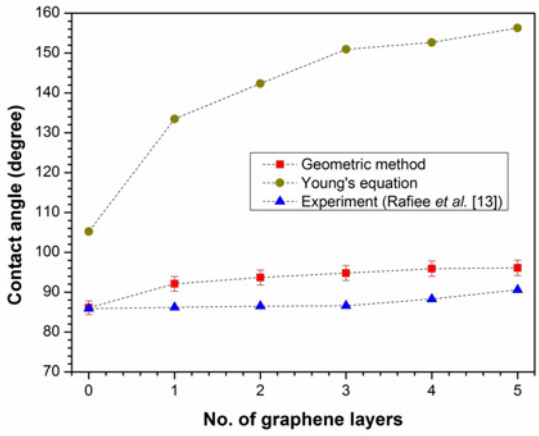

Fig. 6 Contact angles of water droplets obtained from MD simulations Young's equation, and experiments

values (although the increasing tendency of contact angles was the same). This result confirmed that Young's equation is not valid at the nanoscale. Thus, the role of line tension in forming contact angle at nanoscale should be concerned. Overall, for all of the contact angles obtained from the geometric method and the Young's equation, we observed the same phenomenon: the contact angle of the water droplet increased significantly after only a single layer of graphene was coated on the copper substrate. This asserts that depositing a monolayer of graphene on a copper substrate can cause the interaction strength between the substrate and water to decrease drastically.

4. Conclusions

We conducted a series of MD simulations of water droplets on a bare copper substrate and graphene-coated copper substrates. The results showed that by coating a copper substrate with only a single layer of graphene, the contact angle of water droplets is clearly changed. This confirms that there is no wetting transparency for one layer of graphene coated on a copper substrate. Contact angles on the graphene-coated copper substrates gradually increased as the number of graphene layers increased until the contact angle value converged to the value of pure graphite; this occurred with four or more graphene layers. Also, the density profile and stress profile near the substrate-water surfaces were shown to change when more graphene layers were added to the copper substrate. These phenomena demonstrated that the graphene coating reduces the interaction strength between copper and water. The surface tensions at the boundaries between the liquid-vapor, solid-liquid, and solid-vapor were also investigated. Interestingly, the liquid-vapor and solid-vapor surface tensions are almost constant for the different graphene coatings while the solid-liquid surface tension changes; and that confirmed the dominant role of solid-liquid surface tension in forming the contact angles. Additionally, further investigation into the contact angles obtained via Young's equation affirmed its inapplicability at the nanoscale. Most importantly, the results from the water contact angles calculated by the different methods all showed that the contact angles had a tendency to increase as the number of graphene layers coated on the copper substrate increased. This is strong evidence that confirms the significant influence of graphene coating on the wettability of a copper substrate. In conclusion, our study revealed the fact that hydrophobic surfaces can be obtained effectively via graphene coating, which reduces the solid-liquid interaction strength. Also, the contact angle of a liquid on the solid substrate can be changed if the liquid-liquid interaction is changed. However, in this study, the graphene layers used for coating are perfectly smooth. Therefore, a further investigation into coating rough surfaces on a solid substrate should be conducted in order to have a more adequate understanding of the influence of the coating on the wettability of a coated surface.

ACKNOWLEDGEMENT

This research was supported by the Basic Science Research Program through the National Research Foundation of Korea (NRF) funded by the Ministry of Education (NRF-2014R1A1A2057147).

REFERENCES

1. Lee, C., Wei, X., Kysar, J. W., and Hone, J., "Measurement of the Elastic Properties and Intrinsic Strength of Monolayer Graphene," Science, Vol. 321, No. 5887, pp. 385-388, 2008.
2. Bolotin, K. I., Sikes, K., Jiang, Z., Klima, M., Fudenberg, G., et al., "Ultrahigh Electron Mobility in Suspended Graphene," Solid State Communications, Vol. 146, No. 9, pp. 351-355, 2008.
3. Seol, J. H., Jo, I., Moore, A. L., Lindsay, L., Aitken, Z. H., et al., "Two-Dimensional Phonon Transport in Supported Graphene," Science, Vol. 328, No. 5975, pp. 213-216, 2010.
4. Vo, T. Q., Park, B. S., Park, C. H., and Kim, B. H., "Nano-Scale Liquid Film Sheared between Strong Wetting Surfaces: Effects of Interface Region on the Flow," Journal of Mechanical Science and Technology, Vol. 29, No. 4, pp. 1681-1688, 2015.
5. Kim, B. H., Beskok, A., and Cagin, T., "Molecular Dynamics Simulations of Thermal Resistance at the Liquid-Solid Interface," The Journal of Chemical Physics, Vol. 129, No. 17, Paper No. 174701, 2008.
6. Kim, B. H., Beskok, A., and Cagin, T., "Viscous Heating in Nanoscale Shear Driven Liquid Flows," Microfluidics and Nanofluidics, Vol. 9, No. 1, pp. 31-40, 2010.
7. Pham, A. T., Barisik, M., and Kim, B., "Molecular Dynamics Simulations of Kapitza Length for Argon-Silicon and Water-Silicon Interfaces," Int. J. Precis. Eng. Manuf., Vol. 15, No. 2, pp. 323-329, 2014.
8. Pham, A., Barisik, M., and Kim, B., "Pressure Dependence of Kapitza Resistance at Gold/Water and Silicon/Water Interfaces," The Journal Of Chemical Physics, Vol. 139, No. 24, Paper No. 244702, 2013.
9. Vo, T. Q. and Kim, B., "Interface Thermal Resistance Between Liquid Water and Various Metallic Surfaces," Int. J. Precis. Eng. Manuf., Vol. 16, No. 7, pp. 1341-1346, 2015.
10. Rafiee, J., Rafiee, M. A., Yu, Z. Z., and Koratkar, N., "Superhydrophobic to Superhydrophilic Wetting Control in Graphene Films," Advanced Materials, Vol. 22, No. 19, pp. 2151-2154, 2010.
11. Wang, S., Zhang, Y., Abidi, N., and Cabrales, L., "Wettability and Surface Free Energy of Graphene Films," Langmuir, Vol. 25, No. 18, pp. 11078-11081, 2009.
12. Zhou, H., Ganesh, P., Presser, V., Wander, M. C., Fenter, P., et al., "Understanding Controls on Interfacial Wetting at Epitaxial Graphene: Experiment and Theory," Physical Review B, Vol. 85, No. 3, Paper No. 035406, 2012.
13. Rafiee, J., Mi, X., Gullapalli, H., Thomas, A. V., Yavari, F., et al., "Wetting Transparency of Graphene," Nature Materials, Vol. 11, No. 3, pp. 217-222, 2012.
14. Shih, C.-J., Wang, Q. H., Lin, S., Park, K.-C., Jin, Z., et al., "Breakdown in the Wetting Transparency of Graphene," Physical Review Letters, Vol. 109, No. 17, Paper No. 176101, 2012.
15. Raj, R., Maroo, S. C., and Wang, E. N., "Wettability of Graphene," Nano Letters, Vol. 13, No. 4, pp. 1509-1515, 2013.
16. Shin, Y. J., Wang, Y., Huang, H., Kalon, G., Wee, A. T. S., et al., "Surface-Energy Engineering of Graphene," Langmuir, Vol. 26, No. 6, pp. 3798-3802, 2010.
17. Shih, C.-J., Strano, M. S., and Blankschtein, D., "Wetting Translucency of Graphene," Nature Materials, Vol. 12, No. 10, pp.

866-869, 2013.

18. Giovannetti, G., Khomyakov, P., Brocks, G., Karpan, V. v., Van den Brink, J., and Kelly, P., "Doping Graphene with Metal Contacts," Physical Review Letters, Vol. 101, No. 2, Paper No. 026803, 2008.
19. Gao, L., Guest, J. R., and Guisinger, N. P., "Epitaxial Graphene on Cu (111)," Nano Letters, Vol. 10, No. 9, pp. 3512-3516, 2010.
20. Xu, Z. and Buehler, M. J., "Interface Structure and Mechanics between Graphene and Metal Substrates: A First-Principles Study," Journal of Physics: Condensed Matter, Vol. 22, No. 48, Paper No. 485301, 2010.
21. Berendsen, H. J. C., Grigera, J. R., and Straatsma, T. P., "The Missing Term in Effective Pair Potentials," Journal of Physical Chemistry, Vol. 91, No. 24, pp. 6269-6271, 1987.
22. Alejandre, J., Tildesley, D. J., and Chapela, G. A., "Molecular Dynamics Simulation of the Orthobaric Densities and Surface Tension of Water," The Journal of Chemical Physics, Vol. 102, No. 11, pp. 4574-4583, 1995.
23. Allen, M. P. and Tildesley, D. J., "Computer Simulation of Liquids," Oxford Science Publications, p. 164, 1989.
24. Ryckaert, J.-P., Ciccotti, G., and Berendsen, H. J., "Numerical Integration of the Cartesian Equations of Motion of a System with Constraints: Molecular Dynamics of N-Alkanes," Journal of Computational Physics, Vol. 23, No. 3, pp. 327-341, 1977.
25. Mei, J., Davenport, J., and Fernando, G., "Analytic Embedded-Atom Potentials for FCC Metals: Application to Liquid and Solid Copper," Physical Review B, Vol. 43, No. 6, pp. 4653, 1991.
26. Stuart, S. J., Tutein, A. B., and Harrison, J. A., "A Reactive Potential for Hydrocarbons with Intermolecular Interactions," The Journal of Chemical Physics, Vol. 112, No. 14, pp. 6472-6486, 2000.
27. Werder, T., Walther, J. H., Jaffe, R. L., Halicioglu, T., and Koumoutsakos, P., "On the Water-Carbon Interaction for Use in Molecular Dynamics Simulations of Graphite and Carbon Nanotubes," The Journal of Physical Chemistry B, Vol. 107, No. 6, pp. 1345-1352, 2003.
28. Guo, Y. and Guo, W., "Structural Transformation of Partially Confined Copper Nanowires inside Defected Carbon Nanotubes," Nanotechnology, Vol. 17, No. 18, pp. 4726-4730, 2006.
29. Plimpton, S., "Fast Parallel Algorithms for Short-Range Molecular Dynamics," Journal of Computational Physics, Vol. 117, No. 1, pp. 1-19, 1995.
30. Thompson, A. P., Plimpton, S. J., and Mattson, W., "General Formulation of Pressure and Stress Tensor for Arbitrary Many-Body Interaction Potentials under Periodic Boundary Conditions," The Journal of Chemical Physics, Vol. 131, No. 15, Paper No. 154107, 2009.
31. Lopez-Lemus, J. and Alejandre, J., "Thermodynamic and Transport Properties of Simple Fluids using Lattice Sums: Bulk Phases and Liquid-Vapour Interface," Molecular Physics, Vol. 100, No. 18, pp. 2983-2992, 2002.
32. Nijmeijer, M. J. P., Bruin, C., Bakker, A. F., and Van Leeuwen, J., "Wetting and Drying of an Inert Wall by a Fluid in a Molecular-Dynamics Simulation," Physical Review A, Vol. 42, No. 10, pp. 6052-6059, 1990.
33. Nishida, S., Surblys, D., Yamaguchi, Y., Kuroda, K., Kagawa, M., et al., "Molecular Dynamics Analysis of Multiphase Interfaces based on in Situ Extraction of the Pressure Distribution of a Liquid Droplet on a Solid Surface," The Journal of Chemical Physics, Vol. 140, No. 7, Paper No. 074707, 2014.
34. Yuan, Y. and Lee, T. R., "Contact angle and Wetting Properties," Surface Science Techniques, pp. 3-34, 2013.
35. Barisik, M. and Beskok, A., "Wetting Characterisation of Silicon (1, 0, 0) Surface," Molecular Simulation, Vol. 39, No. 9, pp. 700-709, 2013.
36. Voronov, R. S., Papavassiliou, D. V., and Lee, L. L., "Slip length and Contact Angle Over Hydrophobic Surfaces," Chemical Physics Letters, Vol. 441, No. 4, pp. 273-276, 2007.
37. Adamson, A. W., "Physical Chemistry of Surfaces," John Willey & Sons, pp. 183-217, 1990.